Atmos. Chem. Phys. Discuss., doi:10.5194/acp-2015-1008, 2016
Manuscript under review for journal Atmos. Chem. Phys.
Published: 21 January 2016


Atmospheric Chemistry and Physics Discussions

# Diurnal variation of tropospheric relative humidity in tropical region

Isaac Moradi[1,2], Philip Arkin[1], Ralph Ferraro[2], Patrick Eriksson[3], and Eric Fetzer[4]

[1]ESSIC, University of Maryland, College Park, Maryland, USA.
[2]STAR, NOAA, College Park, Maryland, USA.
[3]Chalmers University of Technology, Gothenburg, Sweden.
[4]Jet Propulsion Laboratory (JPL), CalTech, California, USA.

*Correspondence to:* Corresponding author: Isaac Moradi, ESSIC, University of Maryland, College Park, MD 20740, USA. (imoradi@umd.edu)

**Abstract.** Despite the importance of water vapor especially in the tropical region, the diurnal variations of water vapor have not been investigated in the past due to the lack of observations. Measurements from Sondeur Atmosphérique du Profil d'Humidité Intertropicale par Radiométrie (SAPHIR) onboard the low inclination Megha-Tropiques satellite with frequent daily revisits provide a valuable dataset for investigating the diurnal and spatial variation of tropospheric relative humidity in the tropical region. In this study, we first transformed SAPHIR observations into layer-averaged relative humidity, then partitioned the data based on local observation time into 24 bins with a grid resolution of one degree. Afterwards, we fit the Fourier series to the binned data. Finally, the mean, amplitude, and diurnal peak time of relative humidity in tropical region were calculated for each grid point using either the measurements or the Fourier series. The results were separately investigated for different SAPHIR channels as well as for relative humidity with respect to both liquid and ice phases. The results showed that the wet regions are normally associated with convective regions, and the dry regions with the high pressures. The new analysis reveals new findings for the diurnal amplitude and peak time of tropospheric relative humidity. The results showed a large inhomogeneity in diurnal variation of tropospheric relative humidity in tropical region. Although, an early morning peak-time is observed over some parts of tropics, there are significant regions where the diurnal peak time occurs at other times of the day. The results also showed that the diurnal amplitude is less than 10 % in middle and upper troposphere, but it is up to 30 % in lower troposphere over land.

## 1 Introduction

Water vapor is the dominant natural greenhouse gas in the atmosphere, thus it significantly influences the Earth's climate and energy budget. Water vapor is responsible for nearly half of the poleward and most of the upward heat transfer, and also affects the Earth's hydrologic cycle through evaporation and condensation (Sherwood et al., 2010). In addition, water vapor drives extreme weathers such

Atmos. Chem. Phys. Discuss., doi:10.5194/acp-2015-1008, 2016
Manuscript under review for journal Atmos. Chem. Phys.
Published: 21 January 2016


Atmospheric Chemistry and Physics Discussions

as rainstorm, floods, and the initiation of convective cyclones (Keil et al., 2008). Water vapor in the free troposphere, the layer expanding from 1-2 km above the surface up to tropopause, strongly contributes to the water vapor feedback through latent heat and radiation processes (Held and Soden, 2006; Trenberth et al., 2009; Dessler and Sherwood, 2009), with maximum feedback occurring in the tropical free troposphere (Dessler et al., 2008). Additionally, the net cooling of the atmosphere is indirectly affected by tropospheric water vapor through the initiation of clouds and convective heating (Sherwood, 2010). Furthermore, the sensitivity of the Earth's climate to external forcing is enhanced about 70% by water vapor, thus water vapor is also expected to play an important role in global warming and climate change predictions (Cess et al., 1990). For instance, assuming a constant relative humidity (RH) in climate models doubles the rise in temperature compared to when the water vapor feedback is forced to be zero (Minschwaner and Dessler, 2004; Soden et al., 2005).

Most studies in the past have mainly used infrared (IR) satellite data from geostationary orbits to evaluate the diurnal cycle of RH (e.g., Soden, 2000; Tian, 2004; Chung et al., 2007). IR observations are very sensitive to clouds, thus the data need to be strictly filtered for clouds before being analyzed. Therefore, these studies are fundamentally limited to dry conditions because clouds are normally associated with moist regions and cloud screening removes the moist regions from the analysis. One exception is Kottayil et al. (2012) that used multi-instrument microwave measurements from five polar-orbiting satellites to investigate the diurnal variation of brightness temperature (Tb) over the globe. First, polar-orbiting satellites only overpass each location twice a day, thus even a constellation of five satellites do not properly represent the diurnal variation of RH (e.g. see Figure 1 in Kottayil et al. (2012) for the temporal coverage in different years). The orbital drift only slightly enhances the temporal coverage of the data. Second, the multi-instrument differences are an important issue when data are combined. Kottayil et al. (2012) used a dataset that was inter-calibrated using Simultaneous Nadir Observations (SNO). The inter-satellite differences are normally scene dependent, however SNO's normally happen in the polar region so cannot sufficiently resolve the scene dependency due to non-linearity in the calibration of microwave instruments. Additionally, they intercalibrated the Advanced Microwave Sounding Unit-B (AMSU-B) data with respect to the Microwave Humidity Sounder (MHS) instrument. However, due to frequency and polarization differences between the two instruments, the inter-satellite differences are highly non-linear and depend on the atmospheric water vapor content. The observations discussed above are all downward looking, covering altitudes up to about 300 hPa. Diurnal RH variations at higher altitudes have been studied by microwave limb sounding data. Coarse estimates, having a resolution of 6-hour in local time, were provided by Eriksson et al. (2010), by combining data from two different sun-synchronous satellites, Aura Microwave Limb Sounder (MLS) and Odin Sub-Millimeter Radiometer (SMR). These estimates were compared to some climate models and it was found that the models tend to underestimate diurnal variations and partly also simulate maximum RH at wrong local time. Later, Eriksson et al. (2014) derived diurnal variations using the Superconducting Submillimeter-Wave Limb-Emission

Atmos. Chem. Phys. Discuss., doi:10.5194/acp-2015-1008, 2016
Manuscript under review for journal Atmos. Chem. Phys.
Published: 21 January 2016


Atmospheric Chemistry and Physics Discussions

Sounder (SMILES) instrument. SMILES measurements are only available for a 6-month period, but the measurements are made at different local times so suitable for evaluating the diurnal variation. The SMILES data were found to confirm the main features reported by Eriksson et al. (2010).

In summary, despite the importance of water vapor and its distribution in time and space, there still exists a considerable uncertainty in our knowledge of the diurnal and spatial distribution of tropospheric water vapor. The efforts so far have not been able to clearly determine the temporal and spatial distribution of water vapor in the atmosphere due to the lack of observations. This study benefits from observations from Sondeur Atmosphérique du Profil d'Humidité Intertropicale par Radiométrie (SAPHIR) onboard Megha-Tropiques (M-T), a low-inclination satellite with frequent revisits in tropical region between 35 °N and 35 °S. SAPHIR is equipped with six water vapor channels sensitive to upper to lower tropospheric RH. SAPHIR provides a great opportunity to analyze the diurnal and spatial variation of RH in the tropical region using data from a single instrument with an accuracy better than 0.5 K or roughly 5 % in RH space (Moradi et al., 2015a). It is known that diurnal variation of RH is significantly correlated with change in temperature. Therefore, it is more desired to analyze the diurnal variation of absolute humidity parameters. However, measurements from microwave water vapor channels are most sensitive to change in RH and cannot be used to derive absolute humidity parameters. The rest of the paper is organized as follows: Section 2 discusses satellite data used in this study, Section 3 presents the methodology including the satellite Tb to RH transformation method as well as Fourier series, Section 4 discusses the results, and Section 5 summarizes the study.

## 2 Satellite Data

Megha-Tropiques is a low-inclination satellite launched in November 2011 that frequently visits the tropical band between 35 °S and 35 °N. SAPHIR is a microwave humidity sounder onboard the M-T satellite that measures tropospheric RH using several channels centered around the water vapor absorption line at 183 GHz. All SAPHIR channels have double pass-band with horizontal polarization operating at $183 \pm 0.20$, $183 \pm 1.10$, $183 \pm 2.80$, $183 \pm 4.20$, $183 \pm 6.80$, and $183 \pm 11.0$ GHz. The instrument swath width is 1700 km, and the resolution is 10 km at nadir for all the channels. Figure 1 shows the weighting functions for the SAPHIR channels. The peak sensitivity altitude for channels 1-6 respectively changes from upper (almost 6 km) to lower troposphere (nearly 2 km). It should be noted that one limitation of the measurements from microwave humidity sounders is that the peak of Jacobians changes with the water vapor content of the atmosphere. For instance shaded regions in Figure 1 depict the range of Jacobinas for SAPHIR channels derived from the European Organization for the Exploitation of Meteorological Satellites (EUMETSAT) database (Chevallier et al., 2006). However, this shift is expected to be small in tropical region and should not

Atmos. Chem. Phys. Discuss., doi:10.5194/acp-2015-1008, 2016
Manuscript under review for journal Atmos. Chem. Phys.
Published: 21 January 2016


Atmospheric Chemistry and Physics Discussions

affect the results. We used SAPHIR L1A data that are processed by the Centre National d'Etudes Spatiales (CNES).

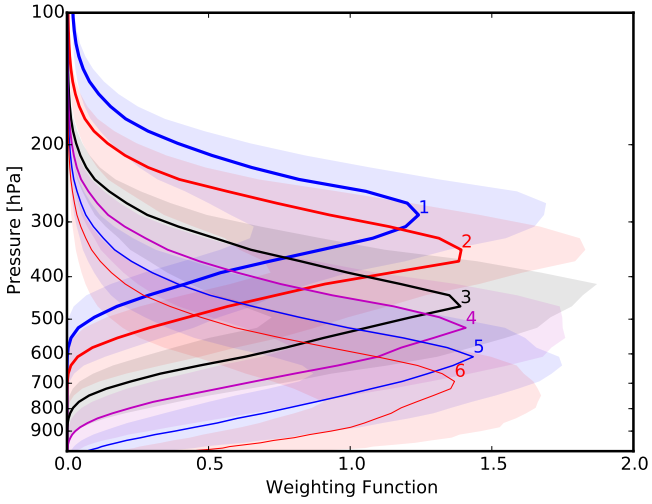


**Figure 1.** The weighting functions for the SAPHIR channels calculated using a subset of EUMETSAT profiles. The selected subset includes 5000 profiles, so that the shaded areas show the range for 25th and 75th percentiles of all profiles. The solid lines show the 50th percentile and the channels' numbers are printed on the plot.

## 3 Methodology

This section discusses the methodology that is used to transform satellite radiances into RH and also Fourier series that are used to investigate the diurnal cycle of tropospheric RH.

### 3.1 Satellite Tb to RH Transformation

A simple method that was developed by Soden and Bretherton (1993) has been widely used in the past to convert satellite microwave measurements to layer averaged RH (e.g., Buehler and John, 2005; Moradi et al., 2010, 2015b). In this simple relation, the satellite Tb's are linearly related to the natural logarithm of layer averaged humidity as follows:

$$ln(RH^{ch}) = a_i^{ch} + b_i^{ch} \times Tb_i^{ch} \quad (1)$$

where $a$ and $b$ are empirical coefficients that change with the earth incidence angle unless the satellite Tb's are corrected for the limb-effect. Since calculating the empirical coefficients as a function of earth incidence angle introduces a very large look-up table; similar to Moradi et al. (2015b), we first applied a limb-correction technique to SAPHIR Tb's then used the same empirical coefficients

Atmos. Chem. Phys. Discuss., doi:10.5194/acp-2015-1008, 2016
Manuscript under review for journal Atmos. Chem. Phys.
Published: 21 January 2016


Atmospheric Chemistry and Physics Discussions

for all the incidence angles. We calculated the limb-darkening ($\Delta Tb$) as the difference between Tb for each beam position and corresponding nadir Tb using data averaged over a long-period of time:

$$Tb^n = Tb(\theta) - \Delta Tb$$
$$\Delta Tb = c \times \ln(cos\theta) \quad (2)$$

where $Tb^n$ is Tb at sub-nadir footprint, and $Tb(\theta)$ is Tb at any given $\theta$ (Moradi et al., 2015b). We preferably used the satellite data to develop the limb-correction technique to avoid any possible errors due to the radiative transfer calculations. As shown in Figure 2, the limb-darkening is stronger for the channels operating near the center of the water vapor absorption line than channels operating near the wings of the line. Figure 2 also shows the values for the coefficient $c$ in Equation 2 for different SAPHIR water vapor channels.

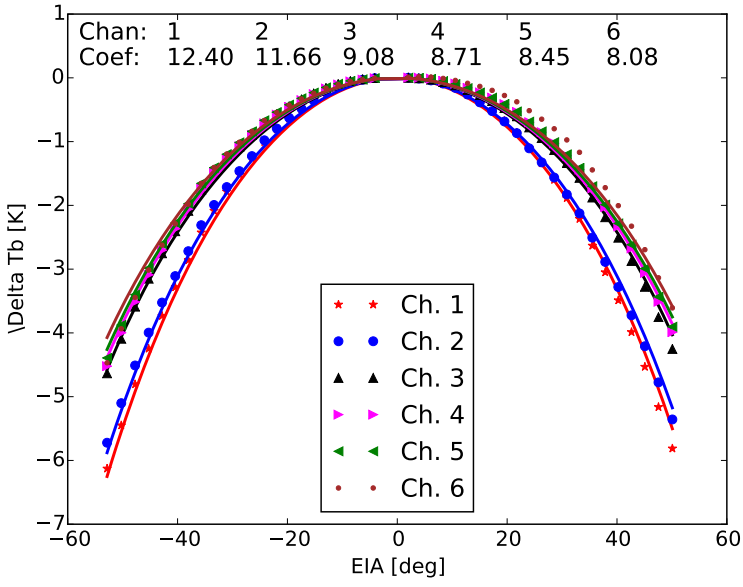


**Figure 2.** Limb-darkening effect as a function of EIA for different SAPHIR channels. The empirical coefficient for Equation 2 are also printed on the plot.

Microwave satellite data are less sensitive to clouds than IR data, however microwave measurements may also be affected by optically thick clouds. Since the empirical coefficients are only valid for clear-sky radiances, the data affected by clouds should be excluded from the analysis. We used the same thresholds proposed by Moradi et al. (2015a) to screen-out the clouds using the differences between Tb's of an upper (Tb5, 183±6.8) and a lower channel (Tb2, 183±1.10). The satellites Tb's are cloud free if $Tb2 - Tb5 < -15$ K and Tb2 $> 240$ K. More details are provided in Moradi et al. (2015a).

Atmos. Chem. Phys. Discuss., doi:10.5194/acp-2015-1008, 2016
Manuscript under review for journal Atmos. Chem. Phys.
Published: 21 January 2016


Atmospheric Chemistry and Physics Discussions

In addition to clouds, some of the satellite radiances may be affected by the surface emissivity which results in low (high) RH values over land (ocean). We used a threshold for Tb's to exclude the measurements that are affected by the surface. Because the emissivity in microwave frequencies is low over ocean (0.5-0.7) and high over land (about 0.9), the Tb's affected by the surface are normally high over land and low over ocean. We used a subset of Atmospheric Radiation Measurement Program (ARM) radiosonde data and also radiative transfer calculations to determine the thresholds for Tb's that are affected by either land or ocean. We performed two set of radiative transfer calculations using the same radiosonde profiles but different emissivity values for land and ocean. Figure 3 shows the Tb's histograms for different SAPHIR channels, when the difference between simulated Tb's for land and ocean is less than $0.01$ K. Therefore, the histograms show the range of Tb's that are not affected by the surface. Based on these histograms we defined the following thresholds for excluding surface affected observations from analysis for channels 1-6, respectively: 230 K to 270 K, 240 K to 280 K, 250 K to 290 K, 255 K to 295 K, 265 K to 295 K, and 270 K to 300 K. The lowest threshold is applied when the observations are affected by the sea surface and the maximum applies when the observations are affected by the land surface. No filter is applied for topography, thus the results over mountainous terrains should be considered with caution since the satellite radiances are averaged over a spatially very inhomogeneous region.

### 3.2 Analyzing Diurnal Variation

Fourier series are traditionally used to model the diurnal cycle of meteorological variables such as temperature and humidity. Fourier series are periodic functions expressed in terms of sine and cosine functions as follows:

$$F(x) = a_0 + \sum_{k=1}^{K} [a_k \cos(kx) + b_k \sin(kx)] \tag{3}$$

where x represents time of the day in radians (x $\in [-\pi, \pi]$) and can be calculated as $x = \frac{t-t_1}{t_1}\pi$, where $t_1$ is equal to 12, $t$ is time of the day in hour, and $a_0$, $a_k$, and $b_k$ are the Fourier coefficients that can be calculated using the following relations:

$$\begin{aligned} a_0 &= \frac{1}{\sum w_i} \sum w_i y_i \\ a_k &= \frac{2}{\sum w_i} \sum w_i y_i \cos(kx_i) \\ b_k &= \frac{2}{\sum w_i} \sum w_i y_i \sin(kx_i) \end{aligned} \tag{4}$$

where $y_i$ are the measurements and $w_i$ indicates the weights given to each measurement. We assume that the data are equally spaced and the points define the middle of each interval, so that $n$ data points can be used to divide the space $[-\pi, \pi]$ into $n$ equal intervals so that $\Delta x = \frac{2\pi}{n}$. Some

Atmos. Chem. Phys. Discuss., doi:10.5194/acp-2015-1008, 2016
Manuscript under review for journal Atmos. Chem. Phys.
Published: 21 January 2016


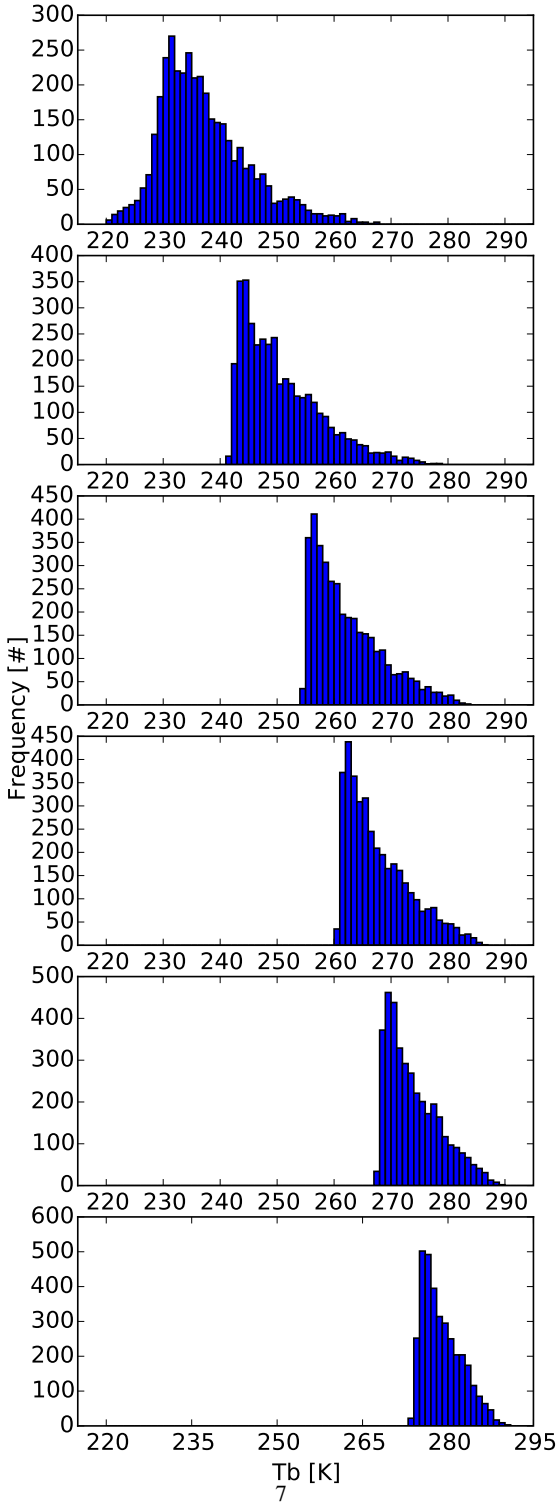


**Figure 3.** Histograms for the distribution of Tb's that are not affected by the surface. The panels from top to bottom are for SAPHIR channel 1 (upper troposphere) to channel 6 (lower troposphere), respectively.

Atmos. Chem. Phys. Discuss., doi:10.5194/acp-2015-1008, 2016
Manuscript under review for journal Atmos. Chem. Phys.
Published: 21 January 2016


Atmospheric Chemistry and Physics Discussions

of the previous studies, e.g., Tian (2004) and Kottayil et al. (2013), have used least square techniques to determine the Fourier coefficients. However, as shown in Equation 4, the coefficients can be mathematically and directly calculated form the measurements. It is also required to determine number of terms that Fourier series should be expanded (i.e., $K$ in Equation 3). However, there is no standard method to determine this number. We evaluated the mean absolute difference between the measurements and the values calculated using Fourier series to determine number of terms that Equation 3 needed to be expanded (see Section 4.4 for more information). It was found out that one term is sufficient over regions with small diurnal variation, but the series needed to be expanded two terms to properly cover the diurnal variation over regions with a larger diurnal amplitude.

## 4 Results

### 4.1 Tb to RH Transformation

We used a subset of the ARM radiosonde data to calculate the empirical coefficients ($a$ and $b$) for Equation 1. Since the saturated vapor pressure can be calculated with respect to either liquid or ice phase, the empirical coefficients can be defined the same way with respect to saturated vapor pressure over either liquid or ice. We use $\mathrm{RH}_I$ to refer to RH with respect to ice and $\mathrm{RH}_L$ for RH over liquid. It is expected that at least for upper tropospheric channels only the ice phase exists. Additionally, for the lower channels the saturated vapor pressure expressions for ice and liquid approach each other. Therefore, in most cases we only present the results for the ice phase ($\mathrm{RH}_I$) and the results for the liquid phase ($\mathrm{RH}_L$) are provided in supplementary materials.

Figure 4 shows an example of the relation between satellite Tb's and natural logarithm of layer averaged $\mathrm{RH}_I$ for SAPHIR channel 2. Channel 2 of SAPHIR operates at $183\pm1$ GHz which is similar to a channel on many humidity sounders such as Advanced Technology Microwave Sounder (ATMS), AMSU-B, and MHS. Therefore, the results can be directly compared with the previous studies. For instance, the coefficients shown in Figure 4 are consistent with Buehler and John (2005), Moradi et al. (2010), and Moradi et al. (2015b).

The empirical coefficients for all the channels are presented in Table 1 with respect to both liquid and ice. Coefficient $a$ for Channel 1 over both ice and liquid is smaller than the same coefficient for other channels, but all other coefficients are very close for all the channels. Both $a$ and $b$ coefficients are greater over ice than over liquid.

### 4.2 Spatial Distribution of RH

SAPHIR observations are available for the tropical region expanding from about 35 S to 35 N. However, we limited the study to the region between 25 S to 25 N, because the frequency of the revisits is limited outside this region. We first binned the data based on local observation time into a grid of $1.0 \times 1.0$ degree. The data-points within each grid-box were gridded into 24 bins based on local

Atmos. Chem. Phys. Discuss., doi:10.5194/acp-2015-1008, 2016
Manuscript under review for journal Atmos. Chem. Phys.
Published: 21 January 2016


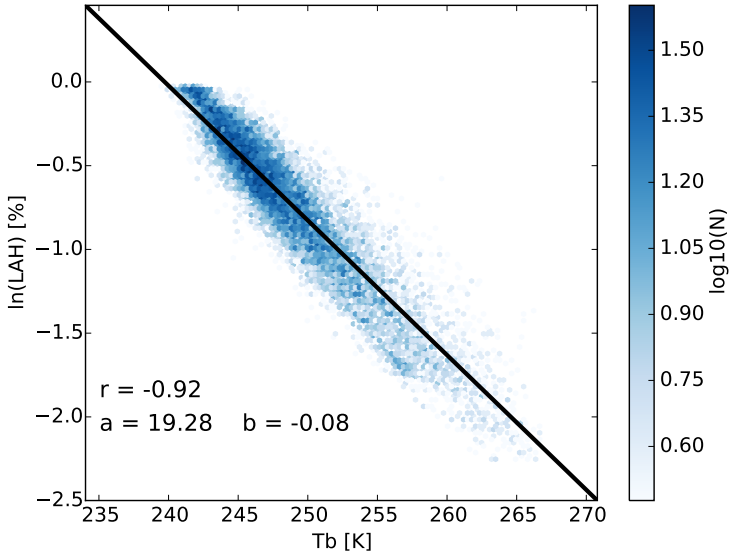


**Figure 4.** Relation between satellite Tb and natural logarithm of layer-averaged $RH_I$. The colorbar shows the logarithm of the number of observations.

**Table 1.** The empirical coefficients for the Tb to RH transformation method for SAPHIR channels.

| | liquid | | ice | |
|---|---|---|---|---|
| Chan. | $b$ | $a$ | $b$ | $a$ |
| 1 | -0.059621 | 13.065021 | -0.067173 | 15.231791 |
| 2 | -0.072363 | 16.974748 | -0.080434 | 19.281791 |
| 3 | -0.063765 | 15.758799 | -0.071711 | 18.022020 |
| 4 | -0.061421 | 15.623266 | -0.069159 | 17.818025 |
| 5 | -0.060818 | 16.033315 | -0.069916 | 18.581239 |
| 6 | -0.061955 | 16.826082 | -0.072675 | 19.818404 |

Atmos. Chem. Phys. Discuss., doi:10.5194/acp-2015-1008, 2016
Manuscript under review for journal Atmos. Chem. Phys.
Published: 21 January 2016


Atmospheric Chemistry and Physics Discussions

observation time. The local time was calculated using Coordinated Universal Time (UTC) and longitude which are both provided in SAPHIR data. Finally, we averaged the data within each grid-box of $1.0^\circ \times 1.0^\circ \times 1.0$ hr. Figure 5 shows average number of observations per hour after the data are filtered for clouds and surface effect. See section 4.3 and Table 2 for details on the boxes shown on the maps. Since the satellite inclination is about 20°, maximum number of observations occurs around 10 °N to 20 °N and 10 °S to 20 °S. After removing the observations that are affected by the surface and clouds, on average, 100 to 300 observations are retained for each bin per hour. Over very high elevations the weighting functions for all the channels peak very close to the surface, therefore, the minimum number of observations occurs over mountains such as the Andes in South America.

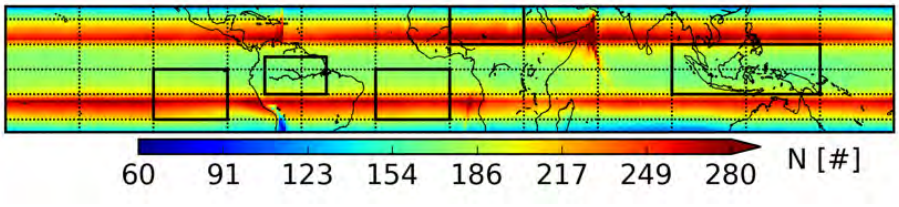


**Figure 5.** Mean number of overpasses per hour for SAPHIR channel 6. Colorbar shows number of observations per grid point. Number of overpasses are generally higher for other channels than for channel 6.

Figure 6 shows the mean daily $RH_L$ for different SAPHIR channels. As expected, RH significantly changes from upper troposphere (14 % to 36 %) to lower troposphere (41 % to 85 % for Channel 6). Note that in order to avoid the outliers especially over the Andes, in most cases, the upper limits printed on the colorbars show the ninety-ninth percentile . The dry regions are observed over high pressures, e.g., South Pacific Ocean, South Atlantic Ocean, as well as Arabian Sea, and are consistent with previous studies (e.g., Moradi et al., 2010; Eriksson et al., 2010). Additionally, several moist regions are observed over convective regions, e.g., South America, Central Africa, and South Asia also known as Maritime Continent which is located within Tropical Warm Pool. The RH generally decreases with distance from the convective regions. The pattern does not change from upper to lower troposphere, but generally the moist region over South Asia is narrower and the gradient is higher in lower troposphere than in upper troposphere. It is also evident that moist regions are connected so that the humidity can be transported across the Equatorial region.

Figure 7 shows the layer-averaged tropospheric $RH_I$. Because the saturated vapor pressure is lower over ice than over liquid, thus the $RH_I$ values are greater than the $RH_L$ values. So that $RH_I$ ranges between 18 % to 52 % in upper troposphere (compared to 14 % to 36 % for $RH_L$), and 38 % to 90 % in lower troposphere (compared to 41 % to 85 % for $RH_L$). Since we excluded the data that are affected by the surface, no difference between land and ocean is observed along the coastlines. The Andes show a large impact on the lower tropospheric RH but a small impact on upper tropospheric RH. The results for regions such as the Andes should be interpreted with cautious because of

Atmos. Chem. Phys. Discuss., doi:10.5194/acp-2015-1008, 2016
Manuscript under review for journal Atmos. Chem. Phys.
Published: 21 January 2016


Atmospheric Chemistry and Physics Discussions

220 uncertainty in the measurements over mountainous regions. The fact that the results do not show a significant land/sea contrast shows that the filter for the surface effect properly removes the surface affected observations.

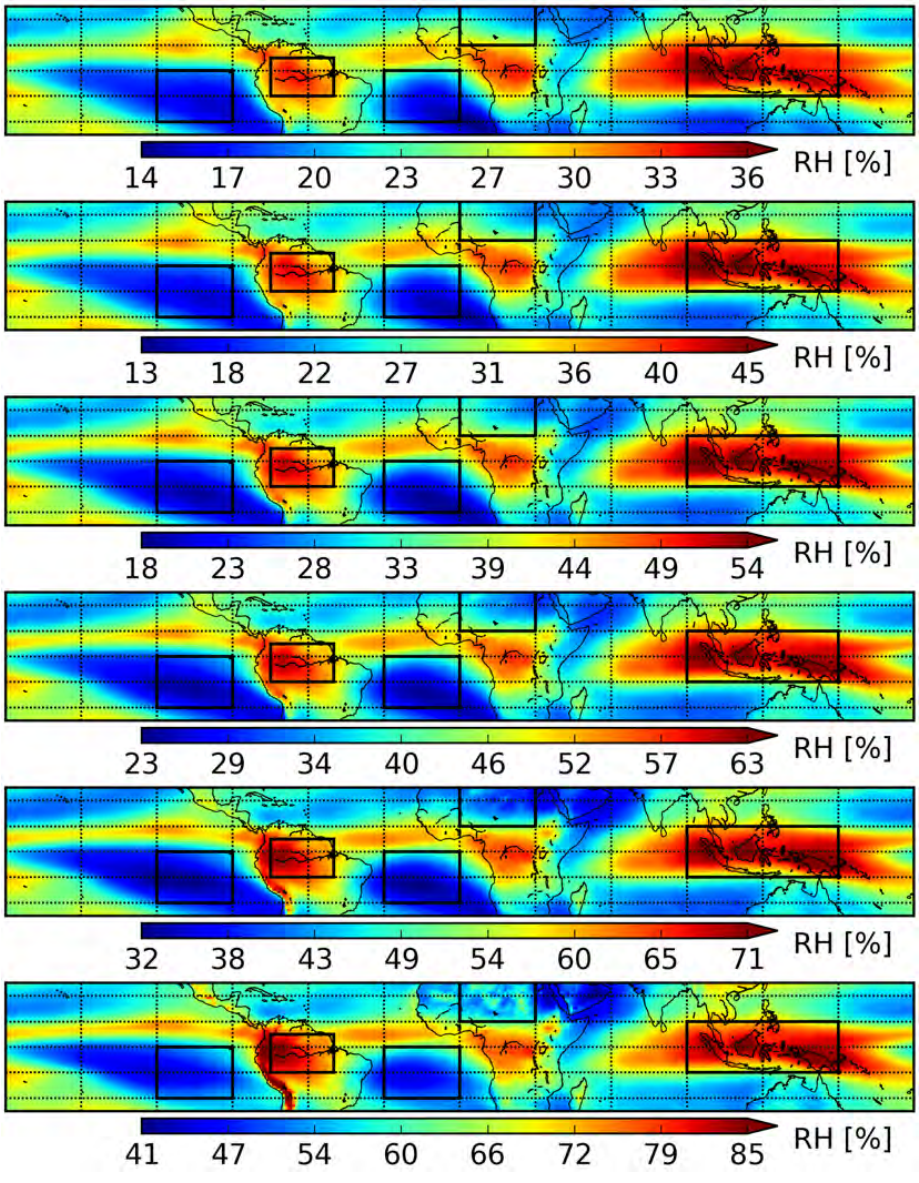


**Figure 6.** Spatial distribution of layer-averaged $RH_L$. Plots from top to bottom are for SAPHIR channels 1-6, respectively.

Atmos. Chem. Phys. Discuss., doi:10.5194/acp-2015-1008, 2016
Manuscript under review for journal Atmos. Chem. Phys.
Published: 21 January 2016


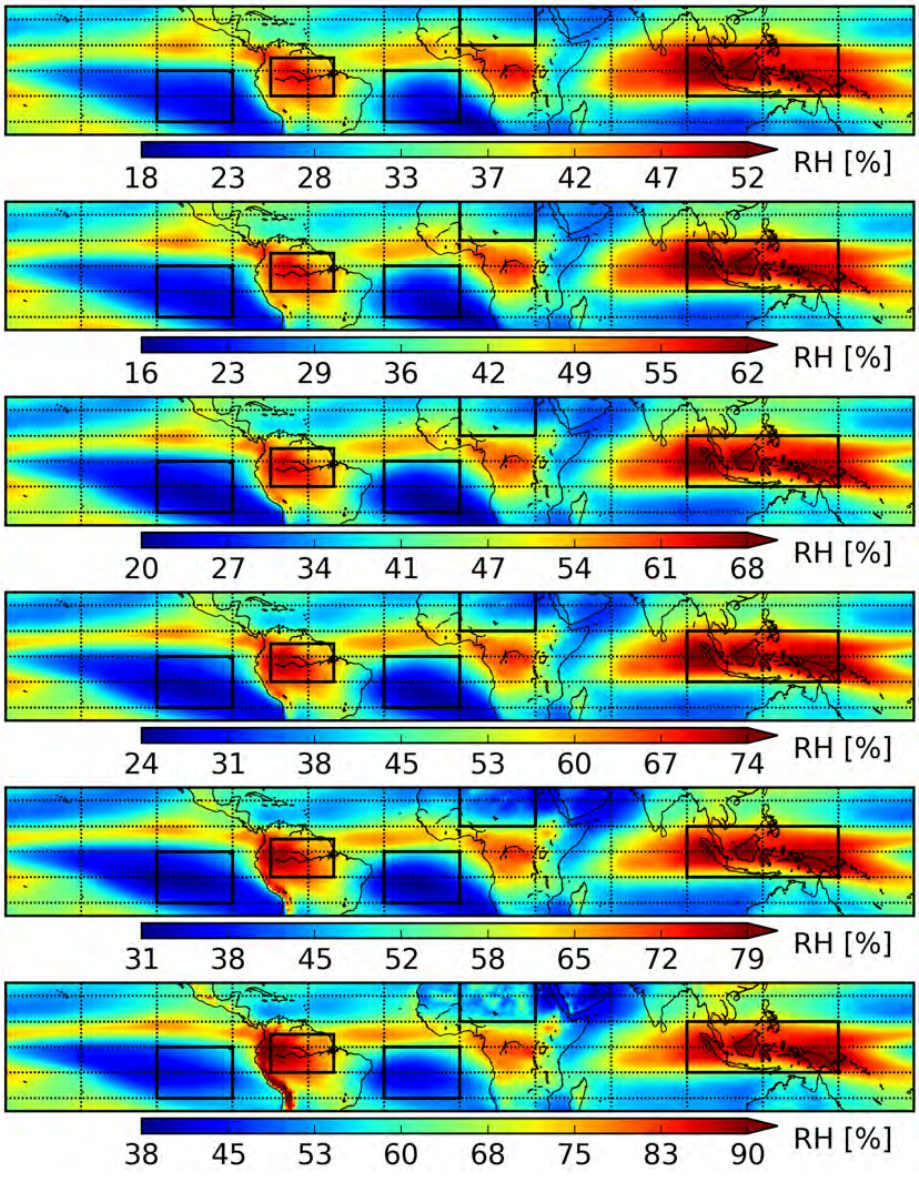


**Figure 7.** Spatial distribution of layer-averaged $RH_I$. Plots from top to bottom are for SAPHIR channels 1-6, respectively.

Atmos. Chem. Phys. Discuss., doi:10.5194/acp-2015-1008, 2016
Manuscript under review for journal Atmos. Chem. Phys.
Published: 21 January 2016


Atmospheric Chemistry and Physics Discussions

Polar orbiting satellites orbit the earth twice a day, thus the daily average of relative humidity estimated from the measurements of these satellites may be biased depending on the crossing time. In order to evaluate the impact of crossing time on the estimated daily averages, we used the observations from only two overpasses being 12 hours apart, similar to ascending and descending orbits of polar-orbiting satellites. We then computed the mean difference of the daily averages calculated using only two overpasses and the daily averages calculated using all the hourly data. Figure 9 shows the results for the measurements from 01:30 (13:30) local time and Figure **??** shows the results for 09:30 (21:30) local time. In fact we collected all the measurement 30 minutes before and after the aforementioned local time. The mid-nigh/afternoon orbit (01:30/13:30 local time) matches with several satellites including NOAA Joint Polar Satellite System and NASA A-Train, and the early morning/late evening orbit (09:30/21:30 local time) matches with the orbit for the MetOp satellites. As shown, especially for the lower tropospheric channels, the error is generally larger for 01:30/13:30 local time, because as shown later, in tropical region the peak of RH generally happens in early morning over many regions. The error is especially considerable for the lower channels when the measurements from 01:30/13:30 local time are used. In both cases, the error is generally less than $2\,\%$ $\mathrm{RH_I}$ in upper troposphere and slightly increases in middle troposphere. However, in lower troposphere the difference between the two cases is considerable. The error due to eliminating diurnal variation is more than $4\,\%$ $\mathrm{RH_I}$ especially over land for the measurements from 01:30/13:30 local time and overall less than $2\,\%$ $\mathrm{RH_I}$ for the measurements from 09:30/21:30 local time. The same figures are included in the supplementary materials for the error in $\mathrm{RH}_L$.

### 4.3 Amplitude and Peak Time

Figure 10 shows the diurnal amplitude of layer-averaged $RH_I$ as the difference between maximums and minimums of RH derived from the Fourier series fit over the course of the day. We employ the diurnal amplitude and peak time derived from the Fourier series, because they are more stable and less noisy than the amplitude and peak time derived from the measurements, though both Fourier series and measurements yield very similar results. The diurnal amplitude derived from the measurements is included in the supplementary materials. No direct relation exist between mean tropospheric RH and the diurnal amplitude. The pattern and magnitude of the amplitude significantly change from upper to lower troposphere. In upper and middle troposphere, i.e., Channels 1-4, the diurnal amplitude is less than $15\,\%$ with the maximum occurring over the Andes, South Africa, Madagascar, and Australia as well as some scattered places over South America and Arabian Desert. The diurnal amplitude in upper troposphere is consistent with Eriksson et al. (2010) who reported up to $8\,\%$ change over tropical land regions in upper troposphere. However, in lower troposphere, the amplitude can be up to $29\,\%$ over land. In lower troposphere, the diurnal amplitude is generally less than $10\,\%$ over ocean, but over deserts and mountains the amplitude is greater than $15\,\%$ with maximum occurring over deserts of South and North Africa, Australia, Middle East, the Andes in South America, and

Atmos. Chem. Phys. Discuss., doi:10.5194/acp-2015-1008, 2016
Manuscript under review for journal Atmos. Chem. Phys.
Published: 21 January 2016


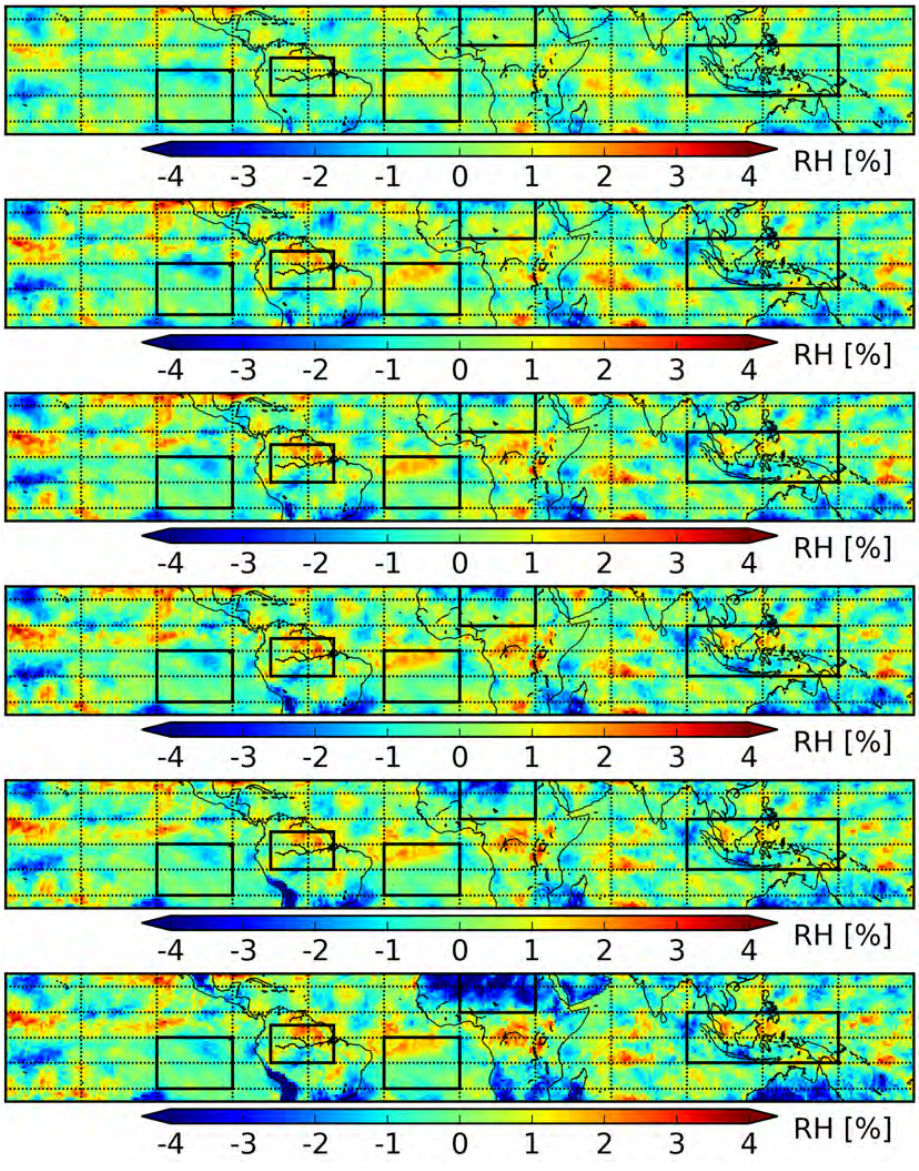


**Figure 8.** Mean difference of daily average of $RH_1$ calculated using only data from 01:30/13:30 local time and the daily average calculated using all hourly data. Plots from top to bottom are for SAPHIR channels 1-6, respectively.

Atmos. Chem. Phys. Discuss., doi:10.5194/acp-2015-1008, 2016
Manuscript under review for journal Atmos. Chem. Phys.
Published: 21 January 2016


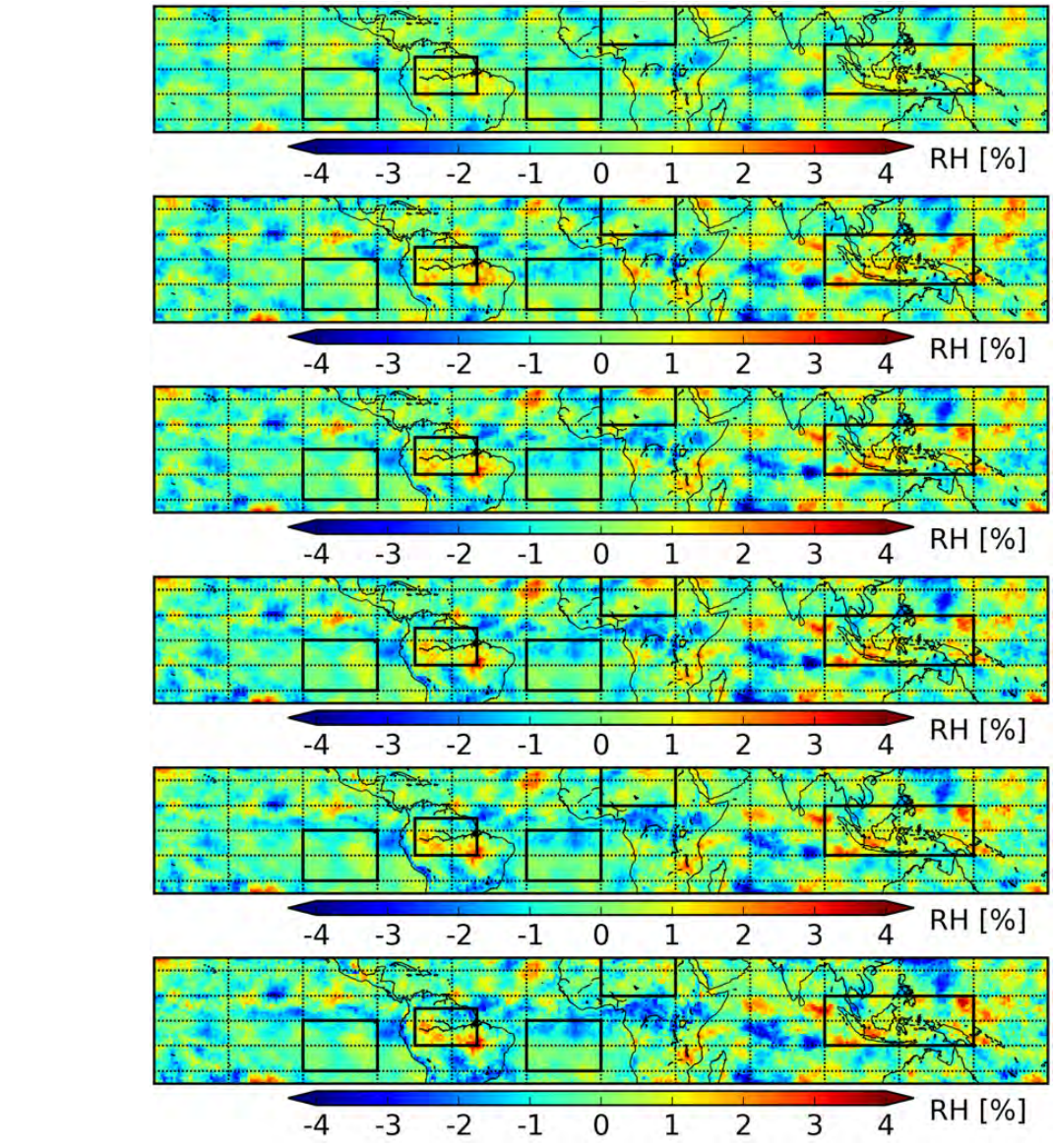


**Figure 9.** Mean difference of daily average of $RH_I$ calculated using only data from 09:30/21:30 local time and the daily average calculated using all hourly data. Plots from top to bottom are for SAPHIR channels 1-6, respectively.

Atmos. Chem. Phys. Discuss., doi:10.5194/acp-2015-1008, 2016
Manuscript under review for journal Atmos. Chem. Phys.
Published: 21 January 2016


Atmospheric Chemistry and Physics Discussions

the Sierra Madres mountains in Mexico. The diurnal amplitude for $RH_L$ (see the supplementary materials) is a few percent smaller than that for $RH_I$ but the pattern is very similar. The amplitude slightly changes from channel 1 to channel 5, but it is much larger for channel 6 than for channel 5 (29 % versus 19 % over land). However, the pattern is very similar for channels 5 and 6. Generally, a stronger diurnal amplitude is found over land than over ocean for the lower channels. This can be explained by the fact that the diurnal variation of RH in the lower layers of the troposphere is enforced by the change in surface and boundary layer temperature which are larger over land than over ocean.

Figure 11 shows the $RH_I$ diurnal peak time for different channels derived from the Fourier series fit. The peak time derived from the measurements is shown in the supplementary materials. One clear feature of RH in tropical region is that the peak time over many regions occurs in early morning hours (03:00-08:00 local time). There exists no clear difference between peak times over land and ocean. Generally, over most regions, the peak time is delayed from upper to lower troposphere. For instance, over South East Pacific the diurnal peak time changes from midnight in the upper troposphere to early morning in the lower troposphere. Over Mid Pacific on the east side of Hawaii (between 150 W to 120 W and 10 N to 25 N) the maximum at all levels occur early afternoon. Over south East Asia and North East Australia the maximum occurs around late afternoon to evening. It should be noted that there is a large uncertainty in estimating the peak time when the diurnal amplitude is very small. Generally, the early morning peak time that has been reported before (e.g., Soden, 2000; Tian, 2004; Chung et al., 2007; Eriksson et al., 2010; Kottayil et al., 2013), only occurs in some regions and it is not common for the entire tropical region. Channel 3 in Kottayil et al. (2013) (middle panel in Figure 5) can be directly compared with channel 2 in this study. Over South America (Amazonian region) both studies show night-time peak time. However, over some other regions, e.g., Indian Ocean, the results are not consistent. We show a peak time before 00:00 LT over most part of Indian Ocean but Kottayil et al. (2013) show night-time (between 00:00 and 02:00 LT). However, the results reported in Kottayil et al. (2013) considerably vary for adjacent pixels which is likely to be due to high noise in the data as data from multiple instruments are combined. We have filtered cloud contaminated data, therefore the results are not dominated by cloud diurnal regime in the tropical region. Since Kottayil et al. (2013) did not exclude the surface affected data, the results for the lower channels cannot be compared.

Based on the mean and diurnal amplitude of RH, five regions are selected that will be used to further investigate some of the results. The coordinates (minimum and maximum of latitudes and longitudes) of these rectangular regions are shown in Table 2. These regions from west to east are located over South Pacific Ocean, Amazon, South Atlantic Ocean, North Africa, and South East Asia. These regions are selected in a way to present a high diversity in diurnal amplitude as well as mean tropospheric RH. The boundaries for these regions are shown on all the maps.

Atmos. Chem. Phys. Discuss., doi:10.5194/acp-2015-1008, 2016
Manuscript under review for journal Atmos. Chem. Phys.
Published: 21 January 2016


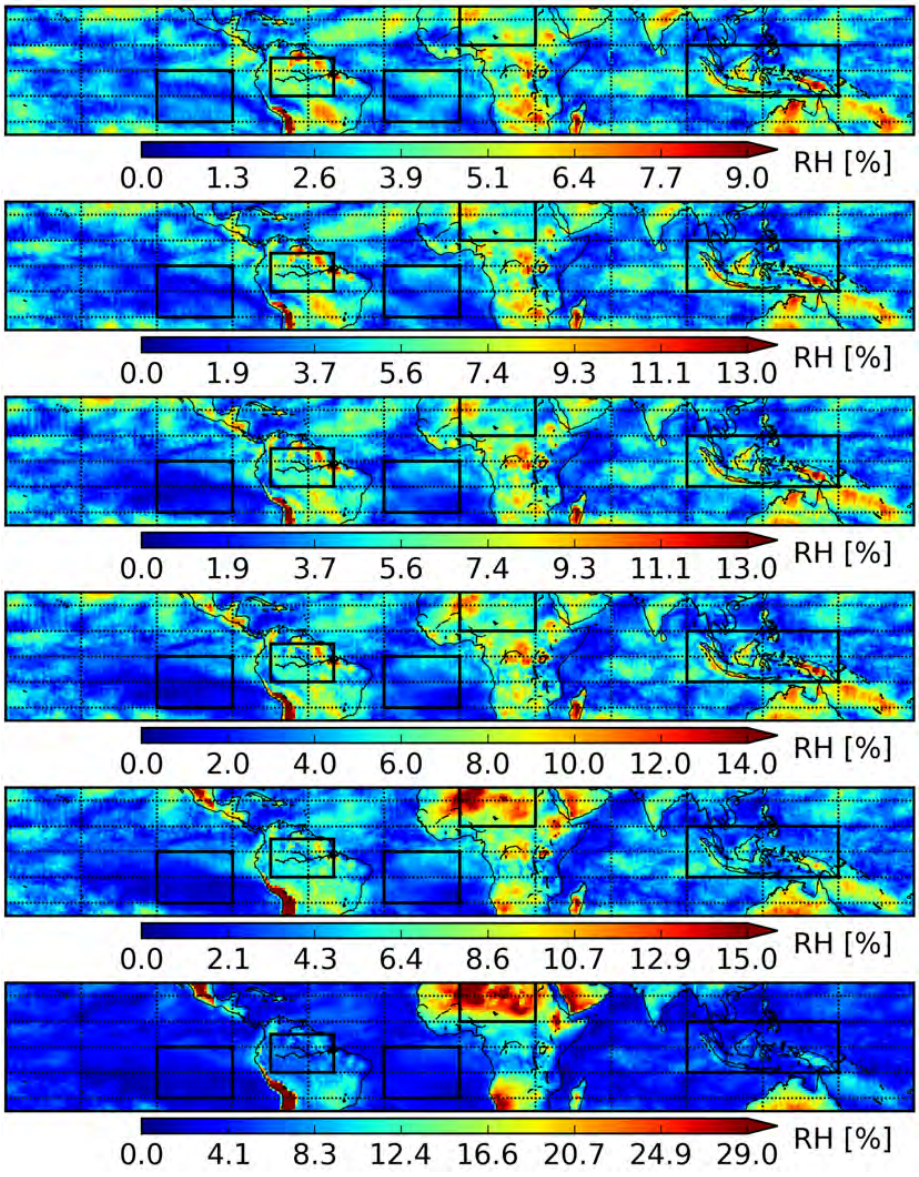


**Figure 10.** Spatial distribution of diurnal amplitude of $RH_I$. Plots from top to bottom are for SAPHIR channels 1-6, respectively.

Atmos. Chem. Phys. Discuss., doi:10.5194/acp-2015-1008, 2016
Manuscript under review for journal Atmos. Chem. Phys.
Published: 21 January 2016


Atmospheric Chemistry and Physics Discussions

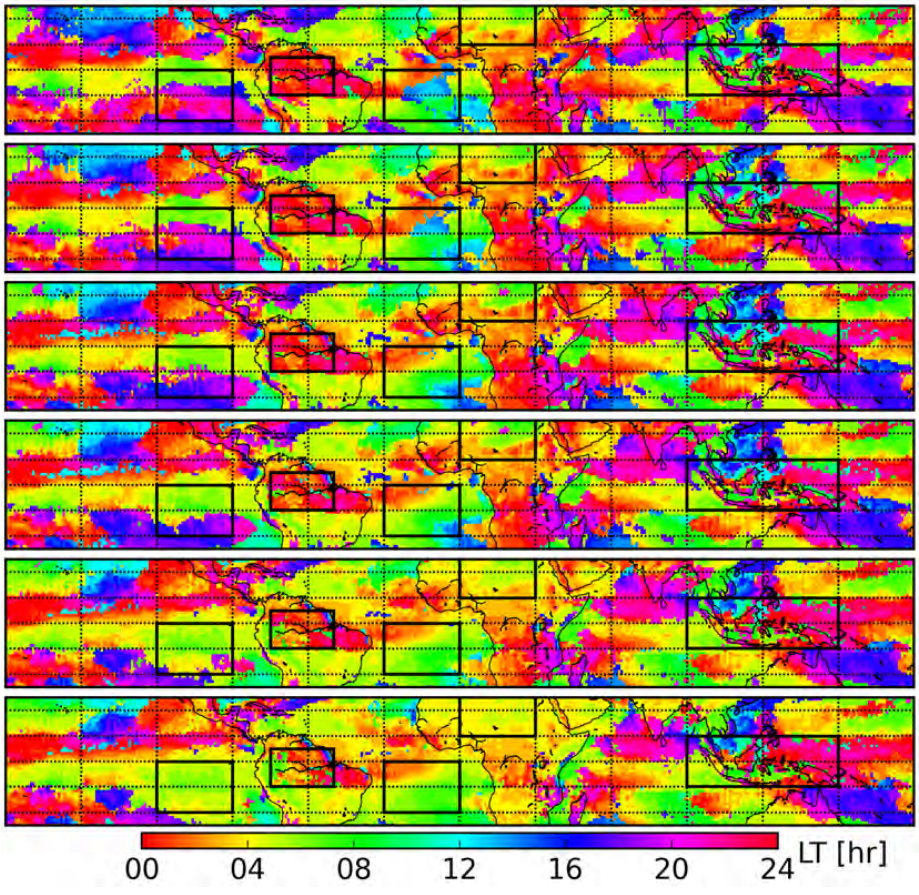


**Figure 11.** Diurnal peak time in local time for $RH_I$ based on Fourier series fit. Plots from top to bottom are for SAPHIR channels 1-6, respectively.

**Table 2.** The regions selected based on mean and amplitude of tropospheric RH to investigate the diurnal variation of RH. The regions are labeled from west to east as South Pacific Ocean (SP), Amazon (AM), South Atlantic Ocean (SA), North Africa (NA), South East Asia (SE), and entire Tropical Region (TR). These regions are indicated on all the maps.

| Label | Lat1 | Lat2 | Lon1 | Lon2 |
|---|---|---|---|---|
| SP | -20 | 0 | -120 | -90 |
| AM | -10 | 5 | -75 | -50 |
| SA | -20 | 0 | -30 | 0 |
| NA | 10 | 25 | 0 | 30 |
| SE | -10 | 10 | 90 | 150 |
| TR | -25 | 25 | -180 | 180 |

Atmos. Chem. Phys. Discuss., doi:10.5194/acp-2015-1008, 2016
Manuscript under review for journal Atmos. Chem. Phys.
Published: 21 January 2016


Atmospheric Chemistry and Physics Discussions

### 4.4 Diurnal Cycle of RH

The diurnal cycle of tropospheric RH is modeled using Fourier series and the series themselves can be demonstrated using the Fourier coefficients. As mentioned before, Fourier series can be theoretically expanded by infinite terms but in practice only a few terms are required for diurnal variation of meteorological variables. In this study, we expanded the Fourier series in only two terms, i.e., k=1,2. As mentioned earlier, this number was determined by analyzing the difference between the measurements and the values estimated using Fourier series. For instance, Figure 12 shows the mean absolute difference between the measurements and the Fourier series fit. Over most regions the difference is less than one percent when the series are expanded in two terms.

Since the coefficient $a_0$ is equal to the mean of the measurements, its distribution is already shown in Figures 6 and 7. The coefficient $a_k$ and $b_k$ present information about the phase and amplitude of the signal and are included in the supplementary materials. If we rewrite the Fourier coefficients as a complex number $z_n = a_n + ib_n$ then the amplitude and phase can be expressed using $|z|$ and $arg(z)$:

$$|z| = \sqrt{zz*} = \sqrt{a^2 + b^2} \tag{5}$$

$$arg(z) = x = tan^{-1}(\frac{b}{a}) \tag{6}$$

where, $arg(z)$ is the phase difference changing from $-\pi$ to $\pi$ and can be converted back to the time of the day using $t = (12x/\pi) + 12$.

In the following, the selected regions will be used to further investigate the diurnal variation of tropospheric RH using Fourier series. Figure 13 shows the diurnal cycle of the layer-averaged $RH_I$ in selected regions for different SAPHIR channels. As shown, in most regions the diurnal amplitude is very small (less than a few percent), but the diurnal amplitude in middle and lower troposphere over North Africa is greater than 10 % (consistent with Figure 10). In upper troposphere (Channels 1 and 2), the diurnal variation is less than 5 % over all selected regions. Over South Pacific, South Atlantic, and North Africa, the maximum RH occurs early morning and the minimum occurs in the afternoon. However, over Amazon and South East Asia the minimum occurs midnight. Over South Atlantic in upper troposphere, the maximum occurs in early afternoon and is shifted to early morning in lower troposphere. As shown in Figure 11, the peak time slightly shifts from upper to lower troposphere. The amplitude over North Africa also changes significantly from a few percent in upper troposphere to more than 20 % in lower troposphere which is due to change in the diurnal variation of air temperature. Figure 11 also includes an example for a grix-box with a large difference between the measurements and the fit for the Fourier series. The grid-box is located near Lago Salar de Arizaro (24.5 °S, 67.5 °W), a small salt flat of the Andes in Argentina. The surface area of the flat is only 1600 $km^2$, therefore the grid-box covers a mix of the salt flat and the surrounding terrains. As shown, the Fourier series are perfectly fitted to the data and the difference between the measurements and the Fourier series fit is rather due to noise in the data.

Atmos. Chem. Phys. Discuss., doi:10.5194/acp-2015-1008, 2016
Manuscript under review for journal Atmos. Chem. Phys.
Published: 21 January 2016


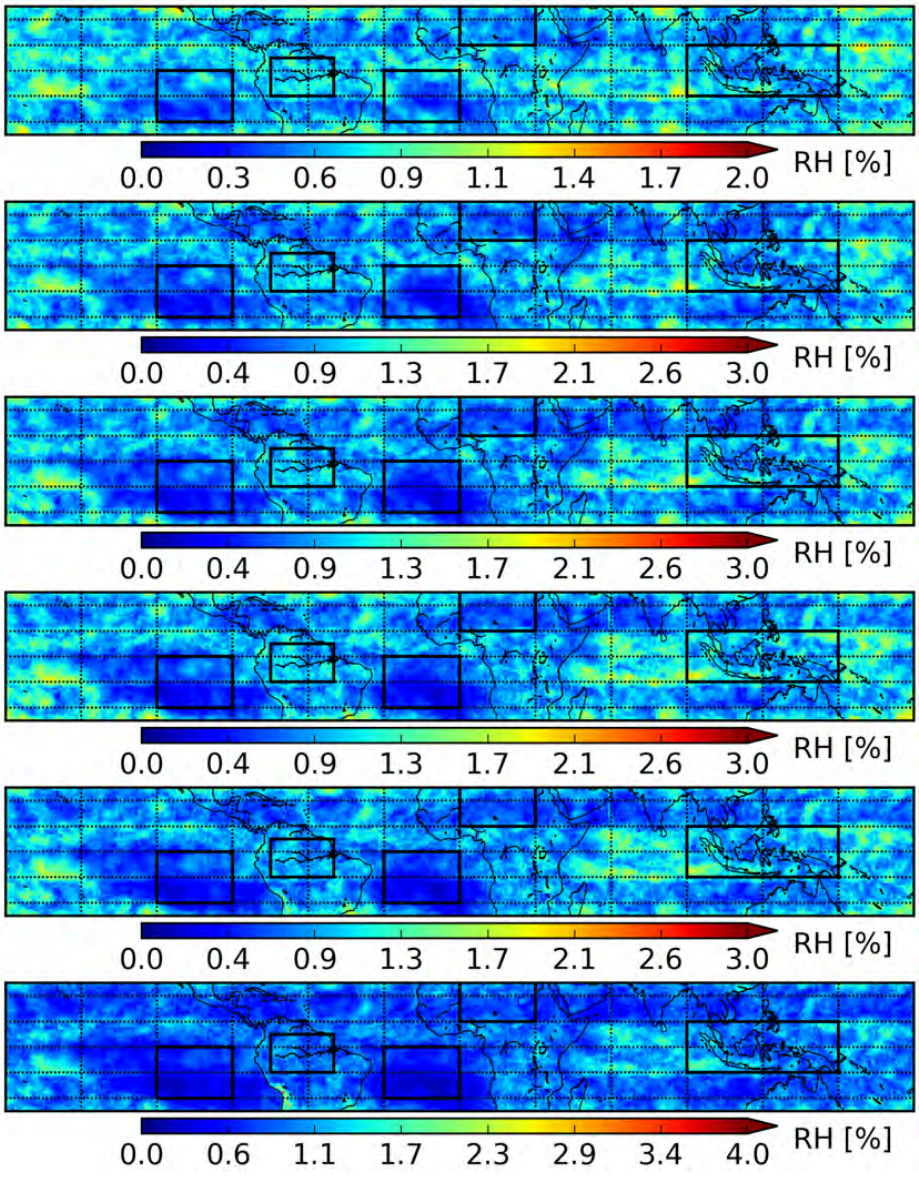


**Figure 12.** Mean absolute difference (with respect to ice) between measurements and the fit for Fourier series. Plots from top to bottom are for SAPHIR channels 1-6, respectively.

Atmos. Chem. Phys. Discuss., doi:10.5194/acp-2015-1008, 2016
Manuscript under review for journal Atmos. Chem. Phys.
Published: 21 January 2016


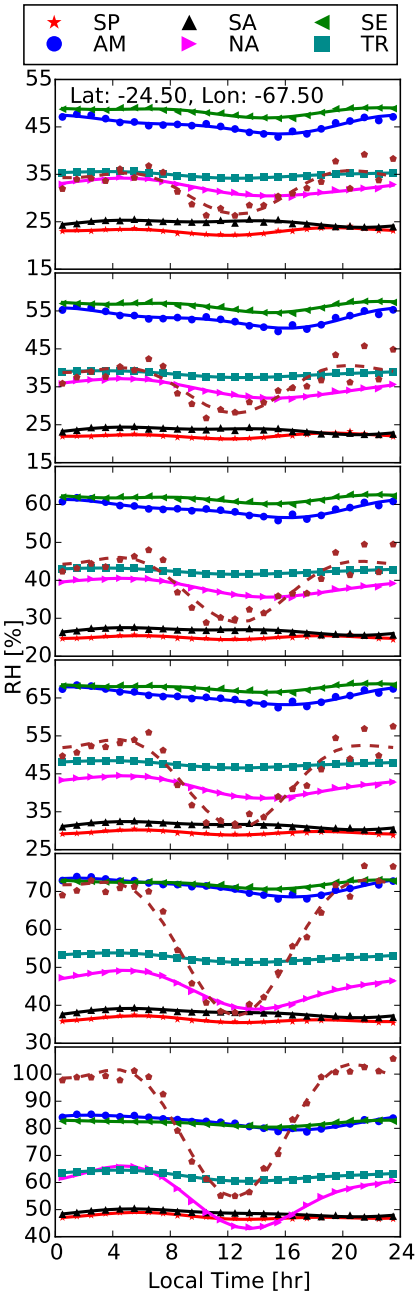


**Figure 13.** Diurnal cycle of layer-averaged $RH_I$ as well as Fourier series fit for the selected regions Plots from top to bottom are for SAPHIR channels 1-6, respectively. The legend shows the name of the regions which are defined in Table 2. The dashed lines show a grid box with a large difference between the measurements (pentagons) and the fit for the Fourier series (the dashed-line). The longitude and latitude of this grid-box are printed on the top plot.

Atmos. Chem. Phys. Discuss., doi:10.5194/acp-2015-1008, 2016
Manuscript under review for journal Atmos. Chem. Phys.
Published: 21 January 2016


Atmospheric Chemistry and Physics Discussions

### 4.5 Distribution Functions

Figure 14 shows the distribution of RH with respect to both liquid and ice over selected regions. In addition the cumulative distribution functions are also provided in the supplementary materials. As shown the distributions of RH with respect to ice and water are similar in the lower troposphere (channels 5 and 6), because the saturation vapor pressure functions approach each other at temperatures above zero. We use RH over ice for channels 1-4, and the over water for channels 5-6. Overall, the distribution functions are very similar for the Amazon and South East Asia regions. Some small differences exist between the two regions especially in the upper troposphere, where South East Asia tend to be more moist than Amazon. The distribution functions are also similar for South Pacific and South Atlantic, but South Atlantic tends to be slightly more moist than South Pacific in all layers. Therefore, we only explain distribution functions for South Atlantic, South East Asia, and North Africa in more detail. The first and third quartiles of the distribution functions are used to explain the range of RH in each layer. The range of RH between first and second quartile include 50% of the data-points. For channel 1, the first (third) quartiles are 15(25), 40 (55), 20 (40), over South Atlantic, South East Asia, and North Africa. None of the regions show a normal distribution function. The distribution is left-skewed (the left tail is longer) for South Atlantic and South East Asia, and right-skewed over the rest of the selected regions. The shape of the distribution remains almost similar for other channels. The quartiles are very similar between channels 1 and 2, but increase about 5% per layer for channels 3 -5. So that the quartiles for each lower channel are about 5% higher than the same quantities for the channel peaking above it. From channels 5 to channel 6, the increase in quartiles is about 10%. Note that in many cases the minimum and maximum are very close to first and third quartile meaning that 25% of the datapoints lie within a small range of RH. Our findings for SAPHIR Channels 1 and 2 are generally consistent with Eriksson et al. (2010), especially for the results presented for AURA-MLS instrument. For instance both studies show that the $RH_I$ can reach up to $80\,\%$ over Africa. However, Eriksson et al. (2010) reported a maximum $RH_I$ of $80\,\%$ to $100\,\%$ over South East Asia but our results show a maximum of $60\,\%$ to $80\,\%$ for SAPHIR Channel 1 and $80\,\%$ to $100\,\%$ for SAPHIR Channel 2. Overall, it is expected that the cloud filter removes some supersaturated regions in our study, because those regions are normally associated with the cloud formation.

### 4.6 Error Estimates

In this section, the error sources are discussed, though it is not possible to quantitatively estimate most of the errors. One obvious source of error is bias and noise in the satellite data. According to Moradi et al. (2015a) the bias in SAPHIR data should be less than $0.5\,\mathrm{K}$ which is roughly equal to $5\,\%$ in RH space. Since a large volume of the data is averaged, the noise in the satellite data should cancel out if the relation between RH and Tb was linear. However, due to the non-linear

Atmos. Chem. Phys. Discuss., doi:10.5194/acp-2015-1008, 2016
Manuscript under review for journal Atmos. Chem. Phys.
Published: 21 January 2016


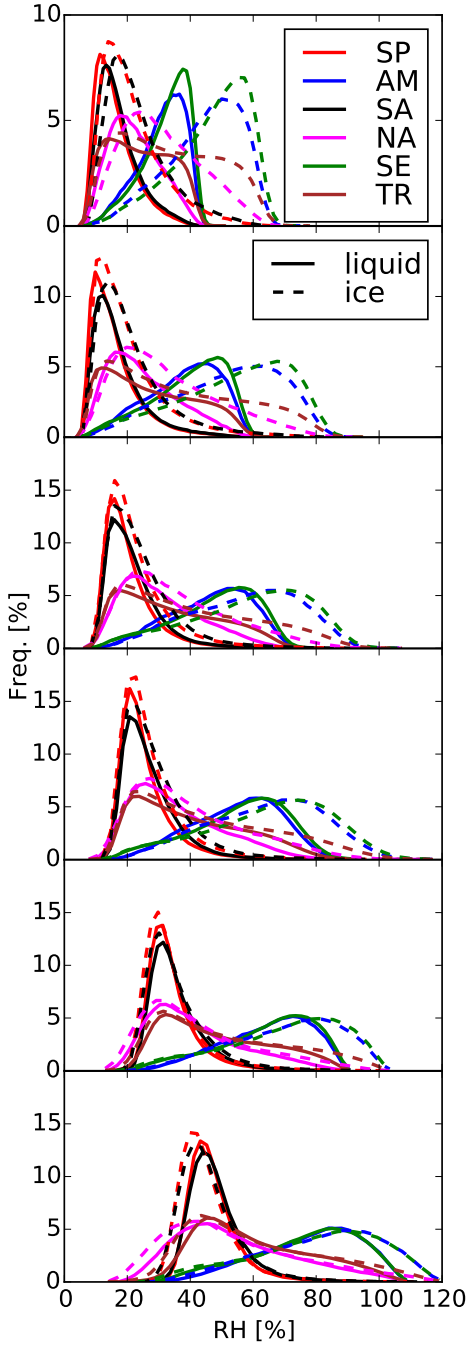


**Figure 14.** Distribution functions for both $RH_I$ and $RH_L$. Plots from top to bottom are for SAPHIR channels 1-6, respectively. The legend shows the name of the regions which are defined in Table 2.

Atmos. Chem. Phys. Discuss., doi:10.5194/acp-2015-1008, 2016
Manuscript under review for journal Atmos. Chem. Phys.
Published: 21 January 2016


Atmospheric Chemistry and Physics Discussions

relation between the two, the random noise may not completely cancel out. Another source of error is from the transformation method which according to Moradi et al. (2015b) is estimated to be less than 10 %. Other sources of error include the surface and cloud effects. Although we have applied appropriate filters, it is still possible that some thin clouds are not filtered out and at least for the lower channels there are still cases that are affected by the surface. The limb-correction technique is based on satellite data averaged over the entire tropics. Therefore, it may introduce at least some noise in the correction for the individual measurements. However, it is expected that the limb-correction does not introduce a systematic bias. The random error introduced by the limb-correction technique may not completely cancel out due to the non-linear between RH and Tb. However, the overall impact of the random error on the results is expected to be negligible. Finally, diurnal variation of RH is highly influenced by change in air temperature, thus sources such as inversion in temperature lapse rate can contribute to the error because satellite data are averaged over a wide layer.

## 5 Conclusions and Summary

Water vapor significantly influences the Earth's climate because of its greenhouse effect. Water vapor is also important to the global water and energy budget. Most of the tropospheric water vapor is concentrated in the tropical region. Additionally, it is estimated that tropical tropospheric humidity significantly contributes to the global warming. Despite this importance, due to the lack of measurements of tropospheric humidity, there is a considerable lack of our understanding of spatial and diurnal variation of tropospheric humidity in tropical region. Most studies, so far have used IR measurements to investigate changes in tropical tropospheric RH, but because of high sensitivity of IR channels to clouds, these studies are significantly biased toward analyzing dry conditions as cloud screening methods remove moist regions from the analysis. Some previous studies have used multi-instrument microwave observations to study diurnal cycle of RH, but due to inter-satellite differences there is a large uncertainty in such studies. SAPHIR is a microwave instrument onboard Megha-Tropiques that provides frequent observations in the tropical region with frequent daily revisits.

In this study, we first transformed the satellite Tb's into layer-averaged RH, then binned the SAPHIR data using the location and local observation time into a grid of $1.0^{\circ} \times 1.0^{\circ} \times 1.0$ hr. Finally, we fitted the Fourier series to the data within each grid-box. The daily-averaged RH values showed that the moist regions are associated with the convective regions and the dry regions are associated with the high pressure regions. The results showed an early morning peak time for most tropical band, but there are significant regions where the peak time occurs over night or in the afternoon. The amplitude significantly changes from upper to lower troposphere especially over lands. So that the maximum amplitude is less than 10 % in upper troposphere but up to 29 % in lower troposphere. The results were analyzed separately for RH with respect to saturated vapor pressure over both ice and

Atmos. Chem. Phys. Discuss., doi:10.5194/acp-2015-1008, 2016
Manuscript under review for journal Atmos. Chem. Phys.
Published: 21 January 2016


Atmospheric Chemistry and Physics Discussions

liquid. The results for both phases are either included in the paper or in the supplementary materials. The analysis shows that microwave measurements from low-inclination satellites are a valuable source for investigating the diurnal and spatial variation of tropospheric RH. The application of the current data is limited to RH as these measurements are most sensitive to the RH than absolute humidity parameters such as specific humidity. The microwave temperature imaging instrument on the same satellite failed shortly after the satellite was launched, otherwise it would have been possible to perform the same analysis for the tropical tropospheric temperature.

## Appendix A: Fourier Series

Fourier coefficients for any known function can be calculated using the following relations:

$$\begin{aligned} a_0 &= \frac{1}{2\pi}\int_{-\pi}^{\pi} f(x)dx \\ a_k &= \frac{1}{\pi}\int_{-\pi}^{\pi} f(x)\cos(kx)dx \\ b_k &= \frac{1}{\pi}\int_{-\pi}^{\pi} f(x)\sin(kx)dx \end{aligned} \tag{A1}$$

The relations presented in Equation A1 are useful when the Fourier series are used to approximate a known function but in our specific case, $f(x)$ is unknown and need to be approximated. These relations can be discretized based on a Riemann sum and the measurements of RH as follows:

$$\begin{aligned} a_0 &= \frac{1}{2\pi}\sum_{i=1}^{n} y_i\Delta x = \frac{1}{n}\sum_{i=1}^{n} y_i = \bar{y} \\ a_k &= \frac{1}{\pi}\sum_{i=1}^{n} y_i\cos(kx_i)\Delta x = \frac{2}{n}\sum_{i=1}^{n} y_i\cos(kx_i) \\ b_k &= \frac{1}{\pi}\sum_{i=1}^{n} y_i\sin(kx_i)\Delta x = \frac{2}{n}\sum_{i=1}^{n} y_i\sin(kx_i) \end{aligned} \tag{A2}$$

In case, different weights are given to the measurements then Equation A1 can be rewritten as shown in Equation 4.

*Acknowledgements.* This study was supported by NOAA grant# NA09NES4400006 (Cooperative Institute for Climate and Satellites - CICS) at the University of Maryland, Earth System Science Interdisciplinary Center (ESSIC). Part of the research was carried out at the Jet Propulsion Laboratory, California Institute of Technology, under a contract with the National Aeronautics and Space Administration. SAPHIR data are processed and provided by Centre National d'Etudes Spatiales (CNES), France. The views, opinions, and findings contained in

Atmos. Chem. Phys. Discuss., doi:10.5194/acp-2015-1008, 2016
Manuscript under review for journal Atmos. Chem. Phys.
Published: 21 January 2016


Atmospheric Chemistry and Physics Discussions

this report are those of the authors and should not be construed as an official National Oceanic and Atmospheric Administration or U.S. Government position, policy, or decision.

Atmos. Chem. Phys. Discuss., doi:10.5194/acp-2015-1008, 2016
Manuscript under review for journal Atmos. Chem. Phys.
Published: 21 January 2016


Atmospheric Chemistry and Physics Discussions

## References

Buehler, S. A. and John, V. O.: A simple method to relate microwave radiances to upper tropospheric humidity, J. Geophys. Res., 110, D02 110, doi:10.1029/2004JD005111, 00053, 2005.

Cess, R. D., Potter, G. L., Blanchet, J. P., Boer, G. J., Del Genio, A. D., Déqué, M., Dymnikov, V., Galin, V., Gates, W. L., Ghan, S. J., Kiehl, J. T., Lacis, A. A., Le Treut, H., Li, Z.-X., Liang, X.-Z., McAvaney, B. J., Meleshko, V. P., Mitchell, J. F. B., Morcrette, J.-J., Randall, D. A., Rikus, L., Roeckner, E., Royer, J. F., Schlese, U., Sheinin, D. A., Slingo, A., Sokolov, A. P., Taylor, K. E., Washington, W. M., Wetherald, R. T., Yagai, I., and Zhang, M.-H.: Intercomparison and interpretation of climate feedback processes in 19 atmospheric general circulation models, J. Geophys. Res., 95, 16 601–16 615, doi:10.1029/JD095iD10p16601, 00776, 1990.

Chevallier, F., Di Michele, S., and McNally, A. P.: Diverse profile datasets from the ECMWF 91-level short-range forecasts, Tech. rep., NWP SAF Satellite Application Facility for Numerical Weather Prediction, 2006.

Chung, E. S., Sohn, B. J., Schmetz, J., and Koenig, M.: Diurnal variation of upper tropospheric humidity and its relations to convective activities over tropical Africa, Atmos. Chem. Phys., 7, 2489–2502, doi:10.5194/acp-7-2489-2007, 2007.

Dessler, A. E. and Sherwood, S. C.: ATMOSPHERIC SCIENCE A Matter of Humidity, Science, 323, 1020–1021, doi:10.1126/science.1171264, 00000 WOS:000263478400028, 2009.

Dessler, A. E., Zhang, Z., and Yang, P.: Water-vapor climate feedback inferred from climate fluctuations, 2003–2008, Geophys. Res. Lett., 35, L20 704, doi:10.1029/2008GL035333, 2008.

Eriksson, P., Rydberg, B., Johnston, M., Murtagh, D. P., Struthers, H., Ferrachat, S., and Lohmann, U.: Diurnal variations of humidity and ice water content in the tropical upper troposphere, Atmos. Chem. Phys., 10, 11 519–11 533, doi:10.5194/acp-10-11519-2010, 00015, 2010.

Eriksson, P., Rydberg, B., Sagawa, H., Johnston, M. S., and Kasai, Y.: Overview and sample applications of SMILES and Odin-SMR retrievals of upper tropospheric humidity and cloud ice mass, Atmospheric Chemistry and Physics, 14, 12 613–12 629, doi:10.5194/acp-14-12613-2014, 2014.

Held, I. M. and Soden, B. J.: Robust Responses of the Hydrological Cycle to Global Warming, Journal of Climate, 19, 5686–5699, doi:10.1175/JCLI3990.1, 2006.

Keil, C., Röpnack, A., Craig, G. C., and Schumann, U.: Sensitivity of quantitative precipitation forecast to height dependent changes in humidity, Geophys. Res. Lett., 35, L09 812, doi:10.1029/2008GL033657, 00016, 2008.

Kottayil, A., Buehler, S. A., John, V. O., Miloshevich, L. M., Milz, M., and Holl, G.: On the Importance of Vaisala RS92 Radiosonde Humidity Corrections for a Better Agreement between Measured and Modeled Satellite Radiances, Journal of Atmospheric and Oceanic Technology, 29, 248–259, doi:10.1175/JTECH-D-11-00080.1, 2012.

Kottayil, A., John, V. O., and Buehler, S. A.: Correcting diurnal cycle aliasing in satellite microwave humidity sounder measurements, Journal of Geophysical Research: Atmospheres, 118, 101–113, doi:10.1029/2012JD018545, 2013.

Minschwaner, K. and Dessler, A. E.: Water Vapor Feedback in the Tropical Upper Troposphere: Model Results and Observations, Journal of Climate, 17, 1272–1282, doi:10.1175/1520-0442(2004)017<1272:WVFITT>2.0.CO;2, 2004.

Atmos. Chem. Phys. Discuss., doi:10.5194/acp-2015-1008, 2016
Manuscript under review for journal Atmos. Chem. Phys.
Published: 21 January 2016




Moradi, I., Buehler, S., and John, V.: Comparing upper tropospheric humidity from microwave satellite instruments and IGRA radiosonde data, in: 2010 11th Specialist Meeting on Microwave Radiometry and Remote Sensing of the Environment (MicroRad), pp. 146–151, doi:10.1109/MICRORAD.2010.5559573, 00001, 2010.

Moradi, I., Ferraro, R., Eriksson, P., and Weng, F.: Intercalibration and Validation of Observations From ATMS and SAPHIR Microwave Sounders, IEEE Transactions on Geoscience and Remote Sensing, PP, 1–1, doi:10.1109/TGRS.2015.2427165, 00000, 2015a.

Moradi, I., Ferraro, R., Soden, B., Eriksson, P., and Arkin, P.: Retrieving Layer-Averaged Tropospheric Humidity From Advanced Technology Microwave Sounder Water Vapor Channels, IEEE Transactions on Geoscience and Remote Sensing, 53, 6675–6688, doi:10.1109/TGRS.2015.2445832, 2015b.

Sherwood, S. C.: Direct versus indirect effects of tropospheric humidity changes on the hydrologic cycle, Environ. Res. Lett., 5, 025 206, doi:10.1088/1748-9326/5/2/025206, 00005, 2010.

Sherwood, S. C., Roca, R., Weckwerth, T. M., and Andronova, N. G.: Tropospheric water vapor, convection, and climate, Rev. Geophys., 48, RG2001, doi:10.1029/2009RG000301, 2010.

Soden, B. J.: The diurnal cycle of convection, clouds, and water vapor in the tropical upper troposphere, Geophys. Res. Lett., 27, 2173–2176, doi:10.1029/2000GL011436, 2000.

Soden, B. J. and Bretherton, F. P.: Upper tropospheric relative humidity from the GOES 6.7 $\mu m$ channel: Method and climatology for July 1987, J. Geophys. Res., 98, 16 669–16 688, doi:10.1029/93JD01283, 00243, 1993.

Soden, B. J., Jackson, D. L., Ramaswamy, V., Schwarzkopf, M. D., and Huang, X. L.: The radiative signature of upper tropospheric moistening, Science, 310, 841–844, doi:10.1126/science.1115602, 00194 WOS:000233121800042, 2005.

Tian, B.: Diurnal cycle of convection, clouds, and water vapor in the tropical upper troposphere: Satellites versus a general circulation model, Journal of Geophysical Research, 109, doi:10.1029/2003JD004117, 2004.

Trenberth, K. E., Fasullo, J. T., and Kiehl, J.: Earth's Global Energy Budget, Bulletin of the American Meteorological Society, 90, 311–323, doi:10.1175/2008BAMS2634.1, 2009.